PROCEEDINGS OF SCIENCE

New Simulations for Ion-Production and Back-Bombardment in GaAs Photo-guns

Josh Yoskowitz*
Old Dominion University
5115 Hampton Blvd, Norfolk, VA 23529, USA
E-mail: yoskowij@jlab.org

J. Grames, J. Hansknecht, C. Hernandez-Garcia, G. A. Krafft, M. Poelker, R. Suleiman
Thomas Jefferson National Accelerator Facility
12000 Jefferson Ave., Newport News, VA 23606 USA

G. Palacios-Seranno, S. Wijethunga
Old Dominion University
5115 Hampton Blvd, Norfolk, VA 23529, USA

S. B. Van Der Geer
Pulsar Physics
Eindhoven, The Netherlands

GaAs-based DC high voltage photo-guns used at accelerators with extensive user programs must exhibit long photo-cathode operating lifetime. Achieving this goal represents a significant challenge for proposed high average current facilities that must operate at tens of milliamperes or more. Specifically, the operating lifetime is dominated by ion back-bombardment of the photo-cathode from ionized residual gas. While numerous experiments have been performed to characterize the operating lifetime under various conditions, detailed simulations of the ion back-bombardment mechanism that explains these experiments are lacking. Recently, a new user routine was implemented using the code General Particle Tracer (GPT) to simulate electron impact ionization of residual beam line gas and simultaneously track the incident electron, secondary electron, and the newly formed ion. This new routine was benchmarked against analytical calculations and then applied to experiments performed at the CEBAF injector at the Thomas Jefferson National Accelerator Facility to study the effectiveness of limiting ions from entering the cathode-anode gap using a positively biased anode. These simulations were performed using detailed 3D field maps produced with CST Microwave Studio describing the photo-gun electrostatics. Discussion of the experiment and the application of this new GPT routine to model the experiments will be presented at the workshop.

The 18th International Workshop on Polarized Sources, Targets, and Polarimetry, PSTP2019
23-27 September, 2019
Knoxville, Tennessee

*Speaker.

PoS(PSTP2019)040

1. Introduction

One of the biggest challenges in creating sustained, high current electron beams in GaAs-based DC high voltage photo-guns is the mitigation of ion back-bombardment [1, 2, 3]. Electrons in the electron beam can ionize residual gas molecules within the photo-gun or within the adjacent beam line. Depending on where they are formed, these positive ions may accelerate towards and bombard the photo-cathode. In the process, these ions can generate secondary electrons or X-rays and desorb gas from the surfaces of vacuum components such as the chamber walls, electrodes and insulators. All of these deleterious ion effects can lead to quantum efficiency (QE) degradation and a decrease in the photo-cathode charge lifetime. Figure 1 below shows the ion back-bombardment process in the CEBAF photo-gun.

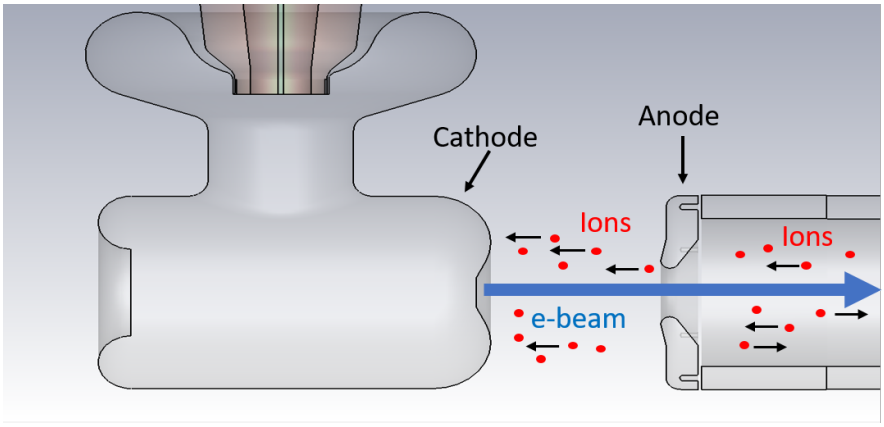

Figure 1: Diagram of the CEBAF Photogun showing the locations of the cathode and anode electrodes. The electron beam ionizes residual gas molecules, which are then accelerated towards the negative potential of the cathode.

The approach we took to hinder ion back-bombardment and increase the lifetime of the photo-cathode is to positively bias the anode. When the anode is biased positively, ions downstream of the anode that would otherwise strike the photo-cathode are instead repelled away from it. This technique has been previously described in [4] and experiments involving a biased anode have previously been performed at Jefferson Lab [5, 6, 7], though detailed simulations of the ion back-bombardment mechanism in the CEBAF photo-gun with a biased anode have not been done prior to this work.

2. Ionization Theory

An electron may produce a positive ion when it scatters off a neutral gas molecule and knocks out one of its own electrons. The incident electron is called the primary electron and the electron ejected from the gas molecule is called the secondary electron. This process is called electron impact ionization and is shown in Figure 2.

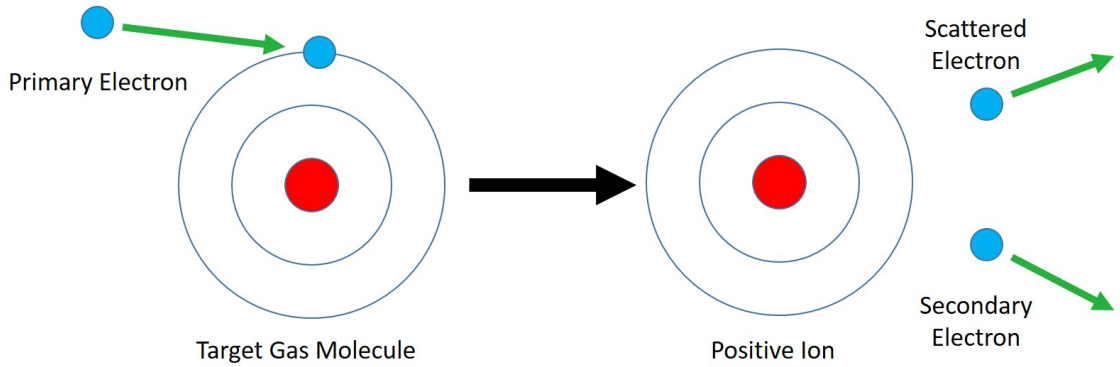

Figure 2: Diagram of electron impact ionization: a beam electron knocks an electron out of a target gas molecule, resulting in a positive ion, secondary electron, and scattered electron.

The probability that an electron will ionize a gas molecule upon collision is given by the ionization cross section (ICS) [8]:

$$\sigma_i\left[\mathrm{m}^2\right] = \frac{1.872\times10^{-24}A_1}{\beta_e^2} f\left(T_e\right)\left[\ln\left(7.515\times10^4 A_2\beta_e^2\gamma^2\right) - \beta_e^2\right] \tag{2.1}$$

$$f\left(T_e\right) = \frac{I_i}{T_e}\left(\frac{T_e}{I_i} - 1\right)$$

$$A_1 = M^2$$

$$A_2 = \frac{e^{\frac{C}{M^2}}}{7.515\times10^4}$$

Here, β_e and γ are relativistic factors for the primary electron, A_1 and A_2 are derived from empirical constants given by Rieke and Prepejchal that depend on the gas species [9], and $f\left(T_e\right)$ is a function for fitting σ at low energies, i.e. when the primary electron kinetic energy T_e is close to the ionization energy I_i of the gas molecule. Only electrons with a kinetic energy greater than the ionization energy I_i of the gas molecule are able to ionize.

Consider a current of electrons I_e moving through a gas of density ρ_i. In a given amount of time Δt, the electrons will move a distance l through the gas. The average ion production rate (IPR) is given by

$$\frac{N_i}{\Delta t} = \rho_i\sigma_i l\frac{I_e}{e} \tag{2.2}$$

Dividing both sides by l, we can write an equation for the IPR per unit length:

$$\frac{N_i}{\Delta t\cdot l} = \rho_i\sigma_i\frac{I_e}{e} \tag{2.3}$$

If we know the number of electrons per unit time passing through the gas instead of the electron current, we can rewrite (2.2) as

$$\frac{N_i}{\Delta t} = \rho_i\sigma_i l\frac{N_e}{\Delta t} \tag{2.4}$$

The average number of ions N_i produced over a given distance l is then

$$N_i = \rho_i\sigma_i l N_e \tag{2.5}$$

Figure 3 below shows the ICS and IPR per unit length for H_2 gas as a function of beam energy and Table 1 below shows calculated values of the ICS and IPR per unit length of H_2 gas for various beam energies.

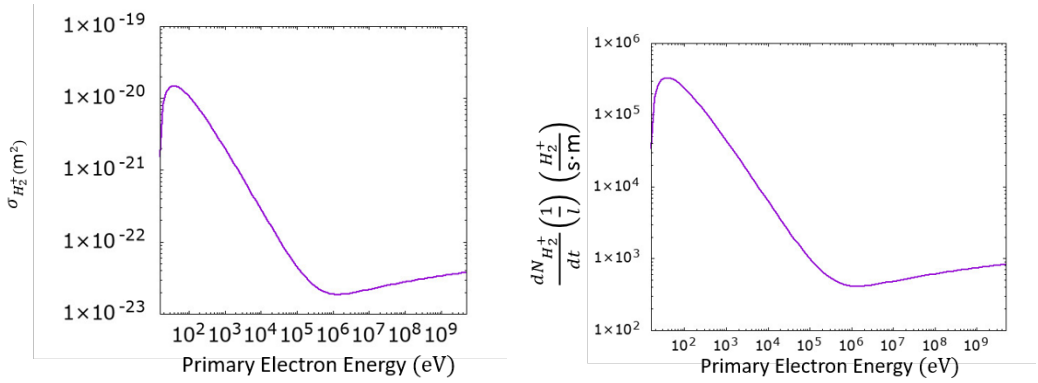

Figure 3: Log-Log plot of the ICS (left) and IPR per unit length (right) as a function of primary electron energy T_e for H_2 gas.

Primary Electron Energy (keV)	$\sigma_{H_2^+}$ (m^2)	IPR $\left(\frac{H_2^+}{\text{s·m}}\right)$
0.1	1.1×10^{-20}	2.4×10^5
1	2.0×10^{-21}	4.4×10^4
10	2.9×10^{-22}	6.3×10^3
100	4.6×10^{-23}	1.0×10^3

Table 1: Calculated values of the ICS and IPR per unit length for H_2 gas assuming $\rho = 3.52 \times 10^{10}$m^{-3} ($10^{-12}$torr) and $I = 100\mu$A.

3. Biased Anode Experiments during 2019 CEBAF Summer Run

3.1 Experimental Setup

The CEBAF photo-gun is constructed with an electrically isolated anode, which allows the anode to be either grounded or biased via a UHV compatible high voltage feedthrough. Figure 4 shows the CEBAF photo-gun with the anode feed-through for biasing. Between June 15th and September 9th of 2019, the CEBAF program required three electron beams to Halls A, B, C respectively with typical total average currents of $70-100\mu$A. Figure 5 shows a plot of the gun current as a function of time for the entire run period. The anode was grounded at the beginning of the run period. We then alternated between biasing the anode at 1kV and grounding it every 2-3 weeks, which corresponded to about $50-60$C of charge extracted from the photo-cathode.

3.2 QE Measurements

QE measurements of the photo-cathode using each of the three lasers were taken every morning for the entire run period. During a QE measurement, the electron beam is stopped briefly, and each laser is incident sequentially on the photo-cathode to produce a small amount of electron

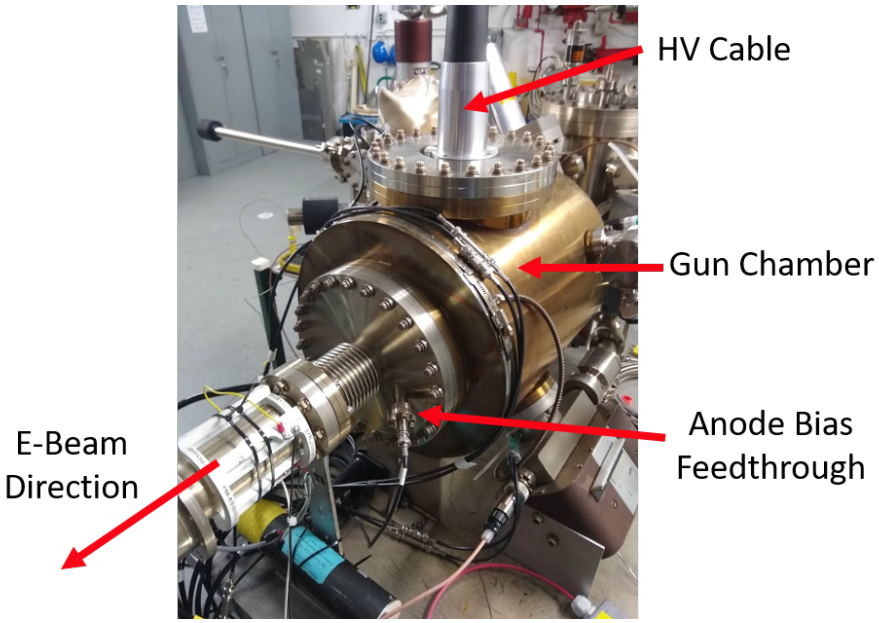

Figure 4: Photo of the CEBAF photo-gun

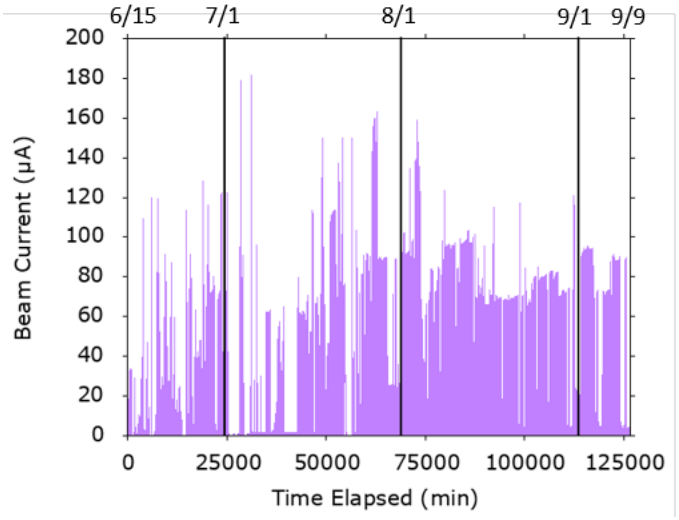

Figure 5: Plot of the electron current extracted from the photo-cathode over the run period.

current I that is measured by a picoammeter. Using each laser's wavelength λ and power P (as measured by a power meter), the QE of the photo-cathode at the laser spot was calculated using the following formula:

$$\begin{aligned} \mathrm{QE} &= \frac{hc}{e}\frac{I}{\lambda P} \\ \mathrm{QE}(\%) &= \frac{124 * I\,(\mathrm{mA})}{\lambda\,(\mathrm{nm})\,P\,(W)} \end{aligned} \tag{3.1}$$

Figure 6 shows all QE measurements for each laser as a function of total charge extracted from the photo-cathode. For each period with the anode either grounded or biased, the QE measurements for each laser were fit with an exponential decay function of the form:

$$\mathrm{QE} = \mathrm{QE}_0 \exp\left(-\frac{q}{\tau}\right) \tag{3.2}$$

Here, τ is the charge lifetime of the photo-cathode: the amount of charge q extracted from the photo-cathode before the QE drops to 1/e of itself. Table 2 lists charge lifetime values for each laser in each anode bias region. To quantify the improvement with the anode biased, Table 3 shows the ratio of the lifetimes between regions 1 and 2 and between regions 3 and 4 for each laser.

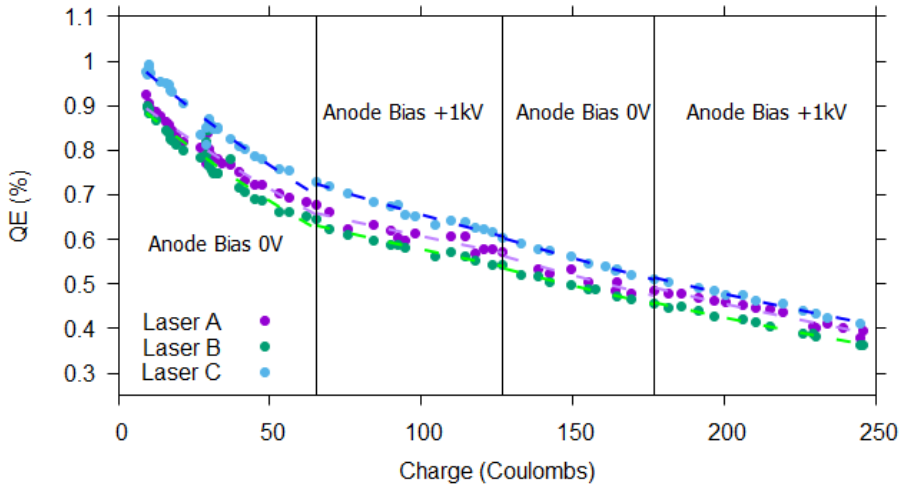

Figure 6: Plot of QE measurements for each laser as a function of the total charge extracted from the photo-cathode. The plot is divided into four regions that correspond to the anode being either grounded or biased. The dots represent QE measurements and the dashed lines represent exponential decay fits to determine the charge lifetime of each laser in each region.

Region	Anode Bias (V)	Laser A Lifetime (C)	Laser B Lifetime (C)	Laser C Lifetime (C)
1	0	181±8	161±9	169±7
2	1000	424±53	392±23	346±16
3	0	288±39	304±14	346±16
4	1000	303±18	302±9	314±11

Table 2: Charge lifetime values for each laser in each anode bias region.

Improvement Ratio	Laser A	Laser B	Laser C
τ_2/τ_1	2.34 ± 0.31	2.43 ± 0.20	2.05 ± 0.13
τ_3/τ_2	0.68 ± 0.13	0.78 ± 0.06	1.00 ± 0.07
τ_4/τ_3	1.05 ± 0.16	0.99 ± 0.05	0.91 ± 0.05

Table 3: Charge lifetime improvement ratios between successive anode bias regions.

3.3 QE Scans of the Photo-Cathode

To gauge the ion bombardment of the photo-cathode, QE scans over the entire photo-cathode active area (not just at the laser spot) were taken before and after the run period, as shown in Figure 7. During a QE scan, one laser is scanned over the surface of photo-cathode in a grid of points covering the active area. At each point, the QE is calculated using equation (3.1). The QE measurements are then interpolated to create smooth contour plots of the QE in the vicinity of the active area. Over the course of the run period, the entire active area experienced QE degradation with the highest amount of degradation at the laser spot.

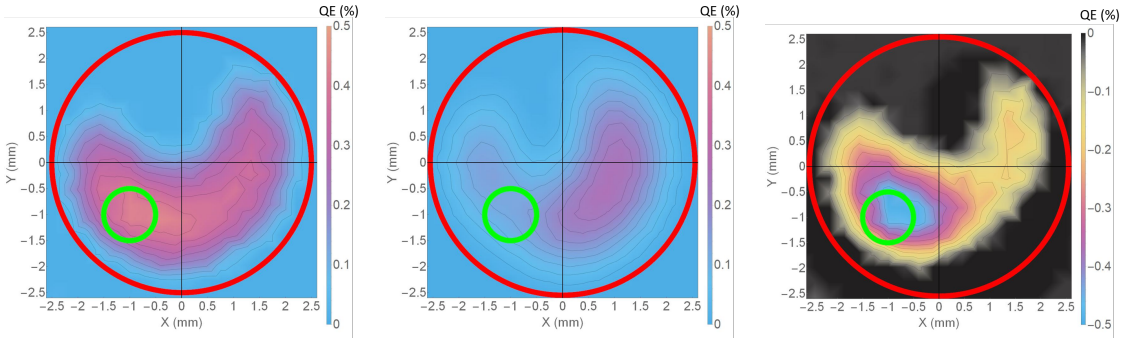

Figure 7: QE scans of the photo-cathode before (left) and after (middle) the 2019 CEBAF Summer run. The red circles denote the 5mm-diameter photo-cathode active area and the green circles denote the 1mm-FWHM laser spot. The plot on the right shows the difference in QE between the two scans.

4. Ion Back-Bombardment Simulations Using GPT

4.1 Initial Particle Distribution

To interpret the measurements performed during the run period, ion simulations were performed using the simulation package General Particle Tracer (GPT) [10]. To generate the initial ion distribution in the GPT simulations, a 0.2pC electron bunch with a 1mm RMS transverse size and 50ps RMS bunch length was tracked up to 0.4m downstream of the photo-cathode. This simulation used a 3D electric field map of the CEBAF photo-gun created using CST Studio Suite software [11] and neglected any space charge effects. Due to the geometry of the cathode electrode, the electrons received a vertical kick downward after leaving the photo-cathode [12]. By dividing the simulation into many timesteps and noting the positions of the electrons at each timestep, a convex volume that surrounds all positions where the electrons in the electron bunch pass through can be created via a 3D convex hull. Since ions can only be created where the electron bunch passes, the

convex hull was uniformly filled with 10^5 macro-particles and was used as the initial particle distribution for the GPT simulations. The number of ions each macro-particle represents was weighted using equation (2.5) and is based on the energy of the electron bunch at the macro-particle's initial location. Hydrogen gas is the predominant gas species in the baked vacuum systems. Thus, for simplicity, it is assumed that only H_2^+ ions are created with the typical CEBAF photo-gun pressure of 10^{-12}torr. The kinetic energy of each ion is equal to the thermal energy at room temperature (293.15K), which corresponds to $T_{H_2^+} = 38$meV, and the direction of each ion after ionization is random. Figure 8 shows the initial spacial distribution of ion macro-particles and Figure 9 shows the total number of ions as a function of distance z from the photo-cathode.

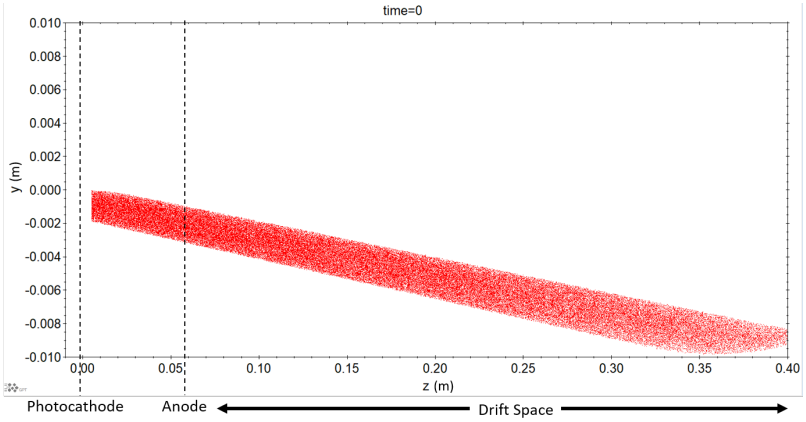

Figure 8: Side-view of the initial ion distribution for GPT simulations. Each red dot represents an individual ion macro-particle.

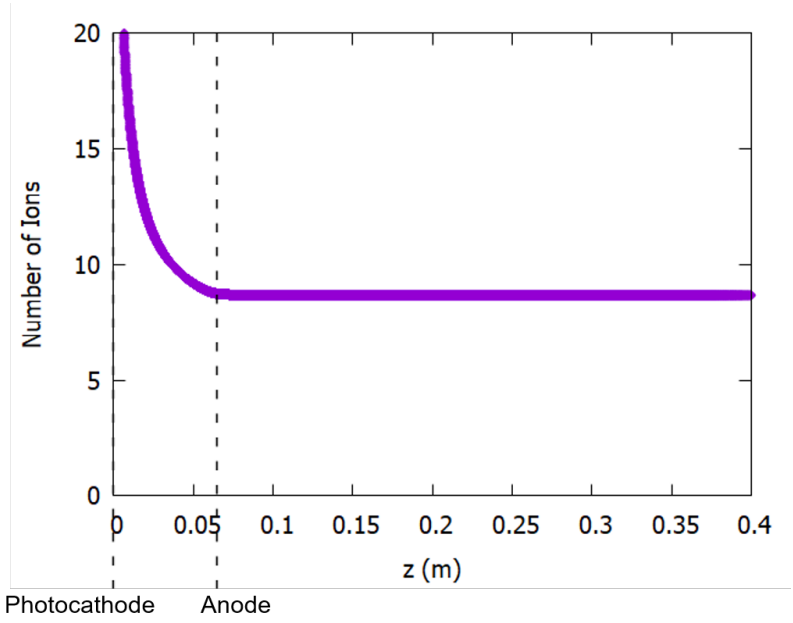

Figure 9: Plot of the initial distribution of ions as a function of distance z from the photo-cathode.

4.2 GPT Simulations

Once the initial ion macro-particle distribution was defined, GPT tracked the movement of ions for a total of 3µs. During the simulations, GPT used a 3D electric field map of the CEBAF photo-gun using a CST model, assuming a -130kV cathode and a 0V anode for the grounded anode simulation or a 1kV anode for the biased anode simulation. Plots of the z-component of the electric field of the photo-gun as a function of z in the grounded and biased anode cases are shown in Figures 10 and 11 respectively. Because the anode bias has a negligible effect on the initial ion distribution, the same initial distribution was used for both simulations. Figure 12 shows the distribution of the ions for the GPT simulations of the grounded and biased anode after 2.25µs.

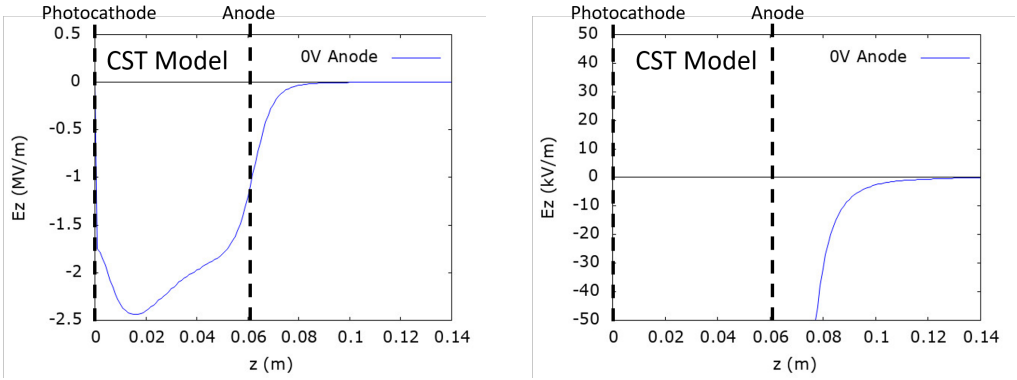

Figure 10: Plots of E_z as a function of z up to 0.14m downstream of the photo-cathode. The left plot shows the entire range of the electric field while the range of the right plot is set to $|E_z| \leq 50\frac{\text{kV}}{\text{m}}$.

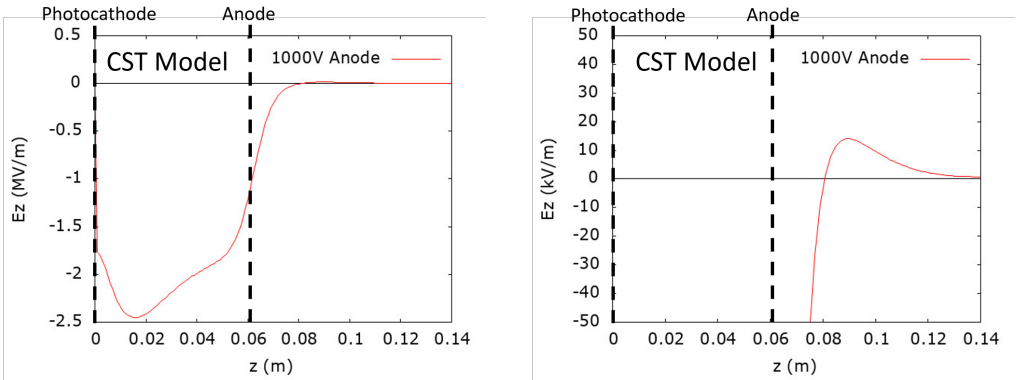

Figure 11: Plots of E_z as a function of z up to 0.14m downstream of the photo-cathode. The left plot shows the entire range of the electric field while the range of the right plot is set to $|E_z| \leq 50\frac{\text{kV}}{\text{m}}$. Note the peak in E_z just after the anode electrode due to the anode bias.

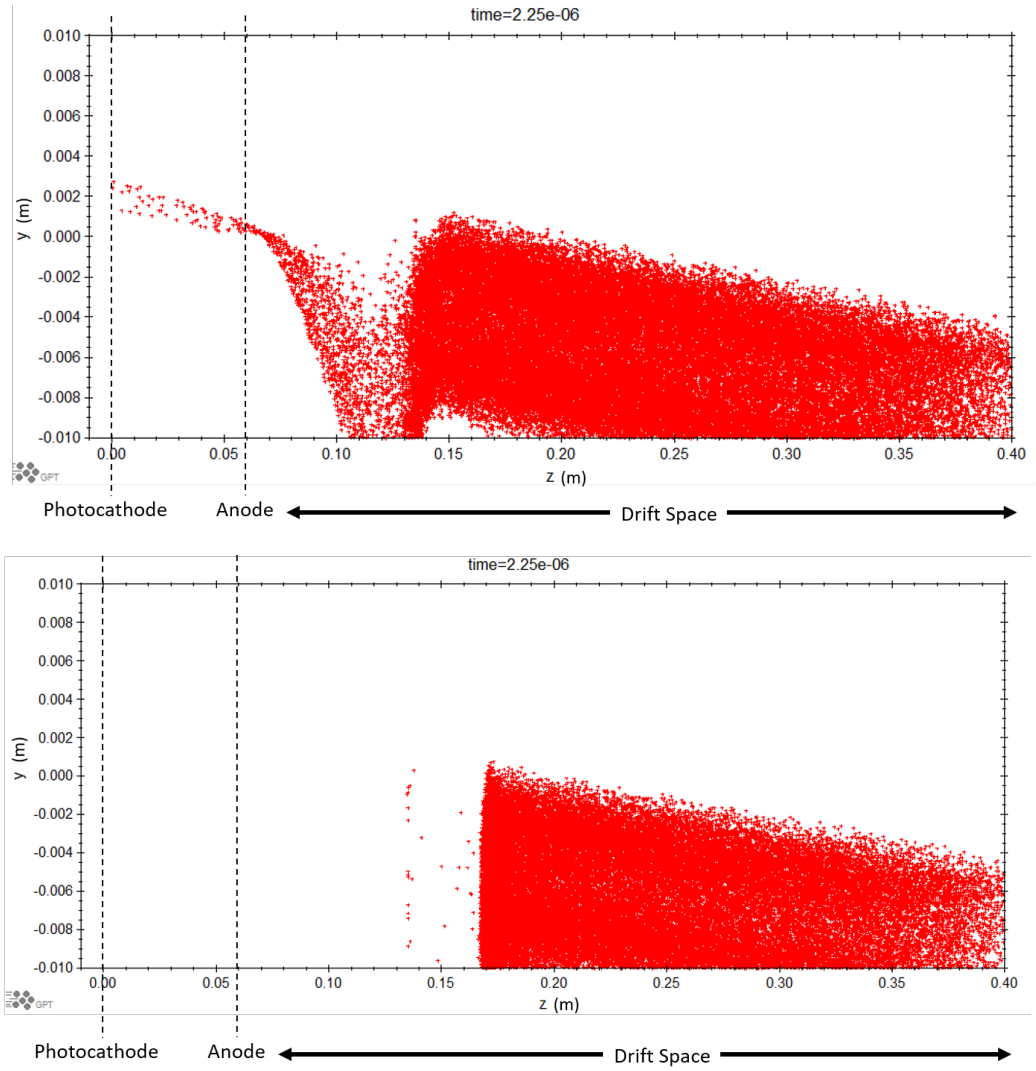

Figure 12: GPT simulations of the CEBAF photo-gun after 2.25μs starting with the initial ion distribution from Figure 8, assuming a −130kV cathode and a 0V anode (top) or a 1kV anode (bottom).

5. Ion Distributions at the Photo-Cathode

During both GPT simulations, the position and energy of all ion macro-particles incident on the photo-cathode were recorded. Figure 13 shows the energy distributions of ions reaching the photo-cathode for a −130kV cathode and a grounded or biased anode. Figure 14 shows number distributions of ions incident on the photo-cathode in the vicinity of the laser spot and Figure 15 shows kinetic energy-weighted number distributions of ions.

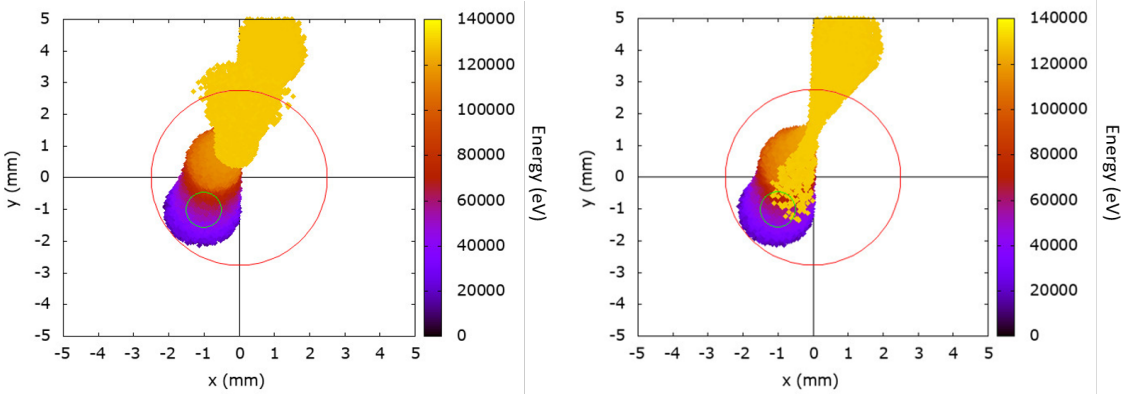

Figure 13: Energy distributions of simulated H_2^+ ions incident on the photo-cathode for a -130kV cathode and grounded anode (left) or biased anode (right). The red circle denotes the 5mm-diameter active area of the photo-cathode and the green circle denotes the 1mm-FWHM laser spot.

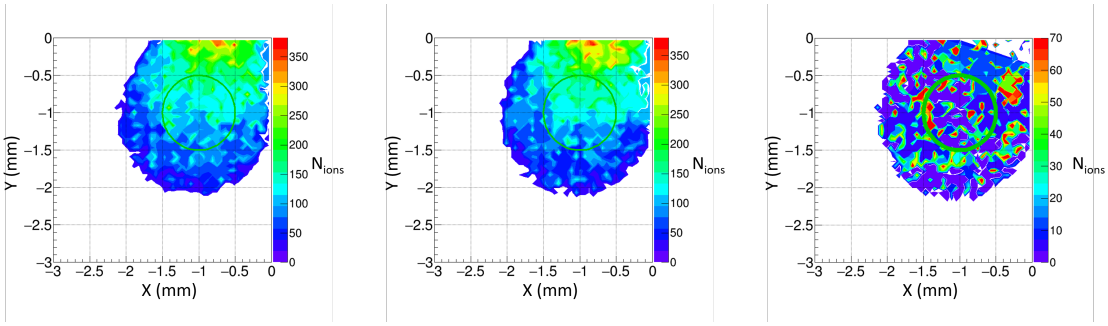

Figure 14: Distributions of simulated H_2^+ ions incident on the photo-cathode in the vicinity of the 1mm-FWHM laser spot (green circle) for a -130kV cathode and grounded anode (left) or biased anode (middle). The plot on the right shows the difference between the grounded anode plot and the biased anode plot.

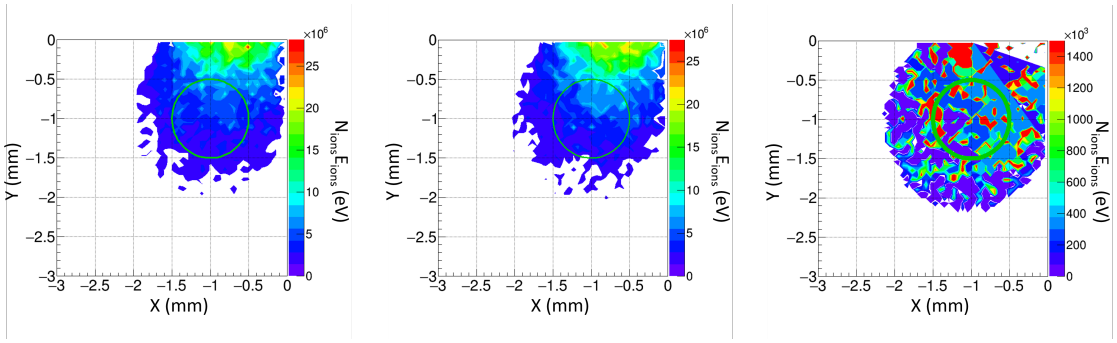

Figure 15: Kinetic energy-weighted distributions of simulated H_2^+ ions incident on the photo-cathode in the vicinity of the 1mm-FWHM laser spot (green circle) for a -130kV cathode and grounded anode (left) or biased anode (middle). The plot on the right shows the difference between the grounded anode plot and the biased anode plot.

6. Discussion

Providing a small, positively biased, ion-repelling field downstream of the photo-gun proved relatively innocuous to implement. This required modifying the downstream 10" flange that supports the anode with a UHV compatible 10kV high voltage feed-through. This modification provides a thin stand-off from the internal fixture of the gun chamber for the anode itself and connects a wire strung with ceramic bushings to complete the electrically isolated circuit. Based on calculations and the electrostatic model, only a small voltage of $1-2$kV is required to provide a sufficient barrier to repel ions with energies running from thermal velocities to the energies gained by the trapping potential of the electron beam. Additionally, measurements characterizing the electron beam (not reported here) indicate no discernible difference in the electron beam size, bunch timing, or energy spread when the anode is biased or grounded.

Comparison of the photo-cathode charge lifetimes in Table 3 indicates a correlation between a biased anode and an improved charge lifetime, suggesting that ion back-bombardment is to some extent mitigated by the presence of the biased anode. It is noteworthy that the relative improvement in the charge lifetime with the anode biased lessens over the course of the study. This interesting feature may be explained in part by: (a) a gradual improvement of charge lifetime independent of the applied bias, which is often observed following a brief reduction in QE after photo-cathode activation when weakly bound states are first removed; (b) the relative exposure of the illuminated photo-cathode area to ions that are within the cathode-anode gap or downstream of it; or (c) the anode bias power supply was found faulted at the end of the run period, which suggests that it may have simply stopped working during the last period.

The simulations of ion tracking and back-bombardment of the photo-cathode in the CEBAF gun are new developments in explaining QE degradation during high voltage beam operation. The application of the tracking program General Particle Tracer and inclusion of detailed 3D field profiles computed by CST Studio Suite demonstrate, as in Figure 12, the utility for sophisticated simulations to model, test and benchmark ion damage. In the grounded anode simulation in Figure 12, we see that ions that are within the cathode-anode gap accelerate towards the photo-cathode and get deflected upward due to the optics of the cathode-anode geometry. In the biased anode simulation, ions within the cathode-anode gap behave similarly to the grounded anode case. However, ions downstream of the anode are repelled away and prevented from passing through the anode and reaching the photo-cathode.

The deflection of incident ions is apparent in Figures 13-15. For both the grounded and biased anode cases, we find the higher the kinetic energy of ions reaching the photo-cathode, the further away from the photo-cathode they originate and the greater their deflection away from the laser spot. That is, ions that are close to the photo-cathode receive the smallest energy gain and thus move straight back towards the laser spot with little to no deflection. Ions that are far from the photo-cathode not only accelerate to a higher energy, but are also focused upward towards the electrostatic center. These simulation results suggest two interesting features for further exploration: (a) the relative spatial pattern of ions striking the photo-cathode reflects the relative spatial reduction in QE measured across the surface of the photo-cathode (see Figure 7) and (b) the relative improvement in photo-cathode lifetime by a factor of 1.5-2 when the anode is biased is most closely correlated with the total number of simulated ions (energy weighted or not) reaching the photo-cathode active

area, compared to those reaching the laser spot itself (see Table 4 below). Development of the model and studies of the ion back-bombardment as a function of the initial conditions are ongoing to improve both accuracy and precision.

Description	Ratio	Value
Total number of ions incident on the PC active area	$\frac{\sum N_{\text{macro,0V}}}{\sum N_{\text{macro,1kV}}} = \frac{4.17\times10^{5}}{2.62\times10^{5}}$	1.59
Total number of ions incident on the PC active area, weighted by incident energy	$\frac{\sum N_{\text{macro}} T_{\text{macro, 0V}}}{\sum N_{\text{macro}} T_{\text{macro, 1kV}}} = \frac{3.99\times10^{10}\text{eV}}{2.03\times10^{10}\text{eV}}$	1.97
Total number of ions incident on the laser spot	$\frac{\sum N_{\text{macro,0V}}}{\sum N_{\text{macro,1kV}}} = \frac{9.45\times10^{4}}{9.51\times10^{4}}$	0.994
Total number of ions incident on the laser spot, weighted by incident energy	$\frac{\sum N_{\text{macro}} T_{\text{macro, 0V}}}{\sum N_{\text{macro}} T_{\text{macro, 1kV}}} = \frac{3.45\times10^{9}\text{eV}}{3.69\times10^{9}\text{eV}}$	0.934

Table 4: Table of improvement ratios quantifying the reduction in ion bombardment using a biased anode instead of a grounded anode. The total number of ions is calculated by counting the number of incident ion macro-particles and summing over the number of ions each macro-particle represents.

7. Ongoing and Future Work

A biased anode has been implemented at the CEBAF injector at Jefferson Lab. Its first operation has demonstrated the capability to improve the photo-cathode charge lifetime and meaningfully extend the useful amount of time Users may receive beam without intervention. The evolution of the improvement with operation is not well understood, but a focus of ongoing research studies.

New simulations using General Particle Tracer were performed to provide insight into the dynamics of ion back-bombardment. The development of a new GPT custom element that includes electron impact ionization is underway to provide realistic dynamical simulations in real time, a feature not currently supported in GPT. As the custom element is developed, there are plans to benchmark against the program IBSimu [13]. Anticipated improvements to the GPT custom element are the inclusion of multiple gas species, secondary electron production, neutral production, and importantly self-consistent space charge effects of the beam potential. The custom element will be used to create more realistic simulations of the CEBAF photo-gun and help to explain the evolution of charge lifetime under various conditions, including the biased anode.

Acknowledgments

This material is based upon work supported by the U.S. Department of Energy, Office of Science, Office of Nuclear Physics under contract DE-AC05-06OR23177. This project has received funding from the European Union's Horizon 2020 research and innovation programme under grant agreement No 824093.

References

[1] K. A. H. G. Andreson et al., *Operating experience with the mami polarized electron source*, in *Proceedings of the Workshop on Photocathodes for Polarized Electron Sources for Accelerators*, D. S. M. Chatwell, J. Clendenin T. Maruyama, ed., SLAC-432, (Stanford, CA), pp. 2–12, 1993.

[2] K. Aulenbacher, *Polarized beams for electron accelerators*, *The European Physical Journal Special Topics* **198** (2011) 361.

[3] J. Grames, P. Adderley, J. Brittian, D. Charles, J. Clark, J. Hansknecht et al., *Ion back bombardment of GaAs photocathodes inside dc high voltage electron guns*, in *Proceedings of the 2005 Particle Accelerator Conference*, pp. 2875–2877, May, 2005, DOI.

[4] E. Pozdeyev, *Ion trapping and cathode bombardment by trapped ions in dc photoguns*, *Phys. Rev. ST Accel. Beams* **10** (2007) 083501.

[5] C. Hernandez-Garcia, P. Adderley, B. Bullard, J. Benesch, J. Grames, J. Gubeli et al., *Compact* -300 kV *dc inverted insulator photogun with biased anode and alkali-antimonide photocathode*, *Phys. Rev. Accel. Beams* **22** (2019) 113401.

[6] J. Grames, P. Adderley, J. Brittian, J. Clark, J. Hansknecht, D. Machie et al., *A biased anode to suppress ion back-bombardment in a dc high voltage photoelectron gun*, *AIP Conference Proceedings* **980** (2008) 110 [https://aip.scitation.org/doi/pdf/10.1063/1.2888075].

[7] J. Grames, R. Suleiman, P. A. Adderley, J. Clark, J. Hansknecht, D. Machie et al., *Charge and fluence lifetime measurements of a dc high voltage GaAs photogun at high average current*, *Physical Review Special Topics - Accelerators and Beams* **14** (2011) .

[8] M. Reiser, *Theory and Design of Charged Particle Beams*. Wiley VCH Verlag GmbH, 2008.

[9] F. F. Rieke and W. Prepejchal, *Ionization cross sections of gaseous atoms and molecules for high-energy electrons and positrons*, *Physical Review A* **6** (1972) 1507.

[10] *General Particle Tracer*, 2019.

[11] *Computer Simulation Technology*, 2019.

[12] G. Palacios-Serrano, F. Hannon, C. Hernandez-Garcia, M. Poelker and H. Baumgart, *Electrostatic design and conditioning of a triple point junction shield for a -200 kv dc high voltage photogun*, *Review of Scientific Instruments* **89** (2018) 104703 [https://doi.org/10.1063/1.5048700].

[13] T. Kalvas, O. Tarvainen, T. Ropponen, O. Steczkiewicz, J. Ärje and H. Clark, *Ibsimu: A three-dimensional simulation software for charged particle optics*, *Review of Scientific Instruments* **81** (2010) 02B703 [https://doi.org/10.1063/1.3258608].